Offline Multiobjective Optimization for Fast Charging and Reduced Degradation in Lithium-Ion Battery Cells Using Electrochemical Dynamics

Fredric Lam, Anirudh Allam, *Graduate Student Member, IEEE*, Won Tae Joe, Yohwan Choi, and Simona Onori, *Senior Member, IEEE*

***Abstract*—The rapid charging of lithium ion battery cells while minimizing degradation is a key challenge in battery management. Offline optimal control frameworks employing physics-based models provide a first-principles approach to this problem that provides critical insights and benchmarks for real-time oriented online optimization algorithms. In this letter, we approach the optimal control problem of minimizing both charging time and degradation of a NMC battery using the single shooting optimization framework, employing a coupled electrochemical-thermal-aging model. The aging mechanism used captures growth of the SEI layer, solvent diffusion. The effectiveness of the single shooting method using a piecewise polynomial control and the low sensitivity of the method to chosen numerical parameters in the multi-objective problem is illustrated. The tradeoff between charging time and degradation is investigated numerically.**

***Index Terms*—Constrained control, energy systems, electrochemical model, optimization.**

I. Introduction

LITHIUM batteries are an important energy storage solution for automotive, grid, and other applications, with the advantages of superior energy efficiency and lifespan [1]. Aside from improvement to battery chemistry, charging strategies that intelligently balance charging speed while avoiding lithium deposition and damage to the battery active material are integral to efficient battery use and battery longevity. Furthermore, constraints on the charging process introduced by safety concerns such as excessive heat generation leading to the possibility of thermal runaway [2] imply additional complexity in the development of charging strategies.

Numerous attempts have been made to compute optimal charging strategies that minimize various combinations of charging time, thermal and aging objectives, using battery models of varying degrees of fidelity. The equivalent circuit model (ECM) has been used to formulate simple optimal control problems (OCPs) with manageable computational effort. The problem of minimizing charging time and energy loss for a simple circuit involving a voltage source and resistor in series is solved analytically in [3], where the optimal strategy is proven to be the well-known constant current, constant voltage (CC-CV) protocol. More complicated circuits involving resistors and capacitors in parallel, however, necessitate the use of numerical solution [3]; in [4], a pseudo-spectral method is applied to an ECM coupled with thermal and aging subsystems to solve a multiobjective problem. The fast charging problem (formulated as a fixed-time, charge-maximization problem) was approached using collocation on a reformulated pseudo-two-dimensional (P2D) model in [5], and using control vector parametrization (CVP) on a similar model in [6]. In [7], CVP was employed to solve the fast charging problem, achieving a significant performance increase relative to CC-CV, and a model predictive control (MPC) strategy was employed in [8] on a simplified ESPM model, with the objective of tracking a fast-charging trajectory. Similarly, MPC was used with a reduced-order model (ROM) to investigate fast-charging subject to no-plating constraints [9]. The multiobjective problem of minimizing charging time and degradation, using a high-fidelity, coupled electrochemical-thermal-aging model, has been introduced by [10], although presently their work is limited to finding suboptimal strategies via dynamic programming. Manual design of charging strategies has also been approached using ROMs [11], although such an approach also does not claim to achieve (local) optimality. To our knowledge, the multiobjective problem minimizing both charging time and degradation has not been attempted using an electrochemical aging model capturing both cycle and calendar degradation.

Manuscript received September 14, 2020; revised November 26, 2020; accepted December 16, 2020. Date of publication December 22, 2020; date of current version March 31, 2021. This work was supported by the LG Chem. Recommended by Senior Editor J.-F. Zhang. *(Corresponding author: Simona Onori.)*

Fredric Lam is with the Institute of Computational and Mathematical Engineering, Stanford University, Mountain View, CA 94040 USA (e-mail: flam@stanford.edu).

Anirudh Allam and Simona Onori are with the Energy Resources Engineering Department, Stanford University, Stanford, CA 94305 USA (e-mail: aallam@stanford.edu; sonori@stanford.edu).

Won Tae Joe and Yohwan Choi are with LG Chem, BMS Advanced SW Project Team, Daejeon 305-738, South Korea.

Digital Object Identifier 10.1109/LCSYS.2020.3046378

TABLE I
SYMBOLS FOR PHYSICAL QUANTITIES

$\mathbf{c}_{s,n}$	Concentration in solid phase (anode) [mol/m^3]	$\mathbf{c}_{s,p}$	Concentration in solid phase (cathode) [mol/m^3]	$\mathbf{c}_{e,n}$	Electrolyte concentration (negative region) [mol/m^3]
$\mathbf{c}_{e,s}$	Electrolyte concentration (separator region) [mol/m^3]	$\mathbf{c}_{e,p}$	Electrolyte concentration (positive region) [mol/m^3]	$\mathbf{c}_{solv}$	Solvent concentration [mol/m^3]
T_c	Cell core temperature [K]	T_s	Cell surface temperature [K]	L_{SEI}	SEI layer thickness [m]
I	Control (applied) current [A]	SOC	State of charge	θ	Stoichiometry
Q	Rated capacity [Ah]	V_{oc}	Cell open-circuit potential [V]	V_{cell}	Cell voltage [V]
t_f	Charging time [s]	C_c	Cell core heat capacity [J/K]	C_s	Cell surface heat capacity [J/K]
R_c	Conductive resistance [K/W]	R_u	Convective resistance [K/W]	i_s	Side reaction current density [A/m^2]
M_{SEI}	SEI layer molar mass [kg/mol]	F	Faraday's constant [C/mol]	ρ_{SEI}	SEI layer density [kg/m^3]
$c_{s,n,min}$	Minimum attainable value of $c_{s,n}$ [mol/m^3]	$c_{s,n,max}$	Maximum attainable value of $c_{s,n}$ [mol/m^3]	$c_{s,p,min}$	Minimum attainable value of $c_{s,p}$ [mol/m^3]
$c_{s,p,max}$	Maximum attainable value of $c_{s,p}$ [mol/m^3]	V_{max}	Maximum permissible cell voltage [V]	T_{amb}	Ambient temperature [K]
U_p	Open circuit potential (cathode) [V]	U_n	Open circuit potential (anode) [V]	η_p	Overpotential (cathode) [V]
η_n	Overpotential (anode) [V]	$\Delta\Phi_e$	Electrolyte potential [V]	R_l	Contact resistance [Ω]
R_{SEI}	SEI layer resistance [Ω]				

In this letter, the direct single shooting method [12], a generalization of the control vector parametrization method [6], is applied to solve a multi-objective optimization problem involving time of charge and degradation. We use an electrochemical-thermal-aging model that quantifies battery degradation via a solid electrolyte interphase (SEI) layer growth model and a solvent diffusion model. The tradeoff in the multiobjective problem involving both charging time and aging objectives is quantified. Furthermore, the efficacy of the single shooting method is demonstrated by the low dimensionality of the resulting optimization problem and scalability to either higher fidelity models or computationally cheaper models.

II. SYSTEM MODEL

ESPM is coupled with a two-state thermal model and an anode SEI layer growth model to describe the dynamics of a single lithium ion cell. The finite difference method is used to discretize the partial differential equations (PDEs) describing solid diffusion, and the finite volume method is used to discretize the electroyte diffusion PDEs, resulting in a system of ordinary differential equations (ODEs) that is in turn coupled with thermal and aging ODEs described in this section. For the sake of brevity, the governing ODE system is provided in a compact form. Explicitly listing the entries for the system matrices in this section along with formulae for state-dependent coefficients would be prohibitively lengthy; the complete system model can be found in [13]. Parameters for the electrochemical and thermal modeling are suited for 18650 battery cells with lithium nickel manganese cobalt oxide (NMC) cathode chemistry, a rated capacity of $Q = 2$ Ah, and a maximum voltage $V_{max} = 4.2$ V. The state vector describing the lithium-ion battery cell is

$$\mathbf{x} = \begin{bmatrix} \mathbf{c}_{s,n} & \mathbf{c}_{s,p} & \mathbf{c}_e & T_c & T_s & L_{SEI} & \mathbf{c}_{solv} \end{bmatrix}^T. \quad (1)$$

The meaning and dimensions of these quantities and those that follow are described in Table I. Note here that bold-faced quantities denote vectors, e.g., $\mathbf{c}_{s,n} = [c_{s,n}^{(1)}, \ldots, c_{s,n}^{(N_r)}]^T \in \mathbb{R}^{N_r}$, where each entry corresponds to nodal or cell-averaged quantities arising from the discretization of the PDEs [13]. Similarly $\mathbf{c}_{s,p} \in \mathbb{R}^{N_r}$, $\mathbf{c}_e = [\mathbf{c}_{e,n}^T, \mathbf{c}_{e,s}^T, \mathbf{c}_{e,p}^T]^T \in \mathbb{R}^{N_{e,n}+N_{e,s}+N_{e,p}}$, and $\mathbf{c}_{solv} \in \mathbb{R}^{N_{SEI}}$, with $N_{e,n} = N_{e,s} = N_{e,p} = N_{SEI} = N_r + 1 = 10$. The length of $\mathbf{x}$ is thus $N_{total} = 2N_r + N_{e,n} + N_{e,s} + N_{e,p} + N_{SEI} + 3 = 61$. The system of ODEs describing the evolution of the state vector results from the discretization methods described in [13] and can be compactly summarized the nonlinear state-space system

$$\frac{d\mathbf{x}}{dt} = \mathbf{f}(\mathbf{x}, u), \qquad \mathbf{x}(0) = \mathbf{x}_0. \quad (2)$$

The scalar control $u \equiv I$ is the current applied to the battery, with $I < 0$ corresponding to charging and $I > 0$ corresponding to discharging.

In the following, (2) is defined in components corresponding to each element in (1), in the order that it appears. The evolution of $\mathbf{c}_{s,n}$ and $\mathbf{c}_{s,p}$ due to diffusion are respectively given by

$$\frac{d\mathbf{c}_{s,n}}{dt} = \alpha_{s,n}(\mathbf{x})A_{s,n}\mathbf{c}_{s,n} + \beta_{s,n}B_{s,n}(I - g_{s,n}(\mathbf{x})) \quad (3)$$

$$\frac{d\mathbf{c}_{s,p}}{dt} = \alpha_{s,p}(\mathbf{x})A_{s,p}\mathbf{c}_{s,p} + \beta_{s,p}B_{s,p}I, \quad (4)$$

where the dependence on the state vector $\mathbf{x}$ is explicitly noted. The functions $\alpha_{s,n}$, $\alpha_{s,p}$, and $g_{s,n}$ are nonlinear functions of the state defined in [13], while $A_{s,n}$, $B_{s,n}$, $A_{s,p}$ and $B_{s,p}$ are fixed matrices.

Similarly, the electrolyte concentration evolution due to diffusion is described by

$$\frac{d\mathbf{c}_e}{dt} = A_e(\mathbf{x})\mathbf{c}_e + B_e(\mathbf{x})I, \quad (5)$$

where solid-electrolyte interface effects [13] are incorporated directly into the matrices A_e and B_e. The core and surface temperatures of the cell are described by the lumped parameters T_c and T_s respectively, and change over time due to overpotential, Joule heating and heat transfer; that is,

$$\frac{dT_c}{dt} = \frac{1}{C_c}\left[(V_{oc}(\mathbf{x}) - V_{cell}(\mathbf{x}))I + \frac{T_s - T_c}{R_c}\right] \quad (6)$$

$$\frac{dT_s}{dt} = \frac{1}{C_s}\left[\frac{T_{amb} - T_s}{R_u} - \frac{T_s - T_c}{R_c}\right] \quad (7)$$

where C_s and C_c are (constant) heat capacities and not to be confused with solid-phase concentrations. Thermal resistances R_u and R_c are fixed.

The anode SEI layer growth used to quantify aging is governed by

$$\frac{dL_{\text{SEI}}}{dt} = -\frac{i_s(\mathbf{x})M_{\text{SEI}}}{2F\rho_{\text{SEI}}}, \tag{8}$$

where i_s is the side reaction current density detailed in [13]. The solvent concentration evolution is given by

$$\frac{d\mathbf{c}_{\text{solv}}}{dt} = A_{\text{solv}}(\mathbf{x})\mathbf{c}_{\text{solv}} + \frac{1}{F}\beta_{\text{solv}}(\mathbf{x})i_s(\mathbf{x})\mathbf{e}_1, \tag{9}$$

where A_{solv} and β_{solv} are state-dependent quantities, and $\mathbf{e}_1 = [1, 0, \ldots, 0]^T$ is used to indicate the boundary term arising due to side reactions.

Other quantities of interest such as the cell state of charge (SOC) and the cell voltage V_{cell} are functions of $\mathbf{x}$ and therefore can be computed directly. Specifically, the state of charge (SOC) of the battery is computed from the bulk-averaged cathode concentration $\bar{c}_{s,p}$ via

$$SOC = \frac{\theta - \theta_{0,p}}{\theta_{100,p} - \theta_{0,p}} = \frac{\bar{c}_{s,p}/c_{s,p,\max} - \theta_{0,p}}{\theta_{100,p} - \theta_{0,p}}. \tag{10}$$

where $\theta_{0,p}$ and $\theta_{100,p}$ are fixed. The cell voltage is computed via $V_{\text{cell}} = U_p + \eta_p - U_n - \eta_n + \Delta\Phi_e - (R_l + R_{\text{SEI}})I$ using quantities defined in Table I; their formulae are found in [13] and [14]. Finally, the open-cell voltage is defined by $V_{oc} = U_p - U_n$. The initial state of the battery $\mathbf{x}_0$ is set such that the initial state of charge $SOC_0 = 0.2$, with spatially uniform concentrations. The temperature is set to equilibrium at the ambient temperature, i.e., $T_c = T_s = T_{\text{amb}}$. The initial SEI layer thickness is fixed at $L_{\text{SEI},0} = 5$ nm.

The time interval of interest is $[0, t_f]$, where $t_f = \inf\{t \geq 0 \mid SOC(t) \geq SOC_{\text{target}}\}$ is the charging time, or time to charge. The quantity $SOC_{\text{target}} = 0.8$ is fixed throughout this letter.

III. Optimal Control Framework

The OCP for fast charging with reduced degradation is defined as follows. We seek the control current I that minimizes the weighted objective function

$$\begin{aligned} J = {} & \alpha\gamma_1 t_f + (1-\alpha)\gamma_2 L_{\text{SEI}}(t_f) \\ & + \gamma_3 |SOC(t_f) - SOC_{\text{target}}| - \sum_{i=1}^{5} \epsilon_i \log f_i \end{aligned} \tag{11a}$$

subject to the dynamics constraints given by (2), and additional inequality constraints

$$\begin{aligned} & c_{s,n,\min} \leq c_{s,n}^{(j)}(t) \leq c_{s,n,\max}, \quad j = 1, \ldots, N_r \\ & c_{s,p,\min} \leq c_{s,p}^{(j)}(t) \leq c_{s,p,\max}, \quad j = 1, \ldots, N_r \\ & V_{\text{cell}}(t) \leq V_{\max}, \\ & \quad I(t) \geq I_{\min}, \quad I(t) \leq I_{\max} \end{aligned} \tag{11b}$$

for all $t \in [0, t_f]$. These inequality constraints are necessary to ensure the solid phase concentrations are physically meaningful at all times and at all positions j, and to keep the cell voltage below a prescribed maximum voltage $V_{\max} = 4.2$ V as is often done in the literature [4], [15]. Simple bounds on the input current $[I_{\min}, I_{\max}] = [-6\text{ A}, -1\text{ A}] = [-3\text{C}, -\text{C}/2]$ are enforced on the control current to prevent over-aggressive charging and to ensure the current remains in the region of validity of the aging model used in [13], which is calibrated on data obtained from experiments with C-rates of -10C to $-$C/2 [14]. The first two terms in (11a) are the fast-charging and aging objective terms, weighed by the tradeoff parameter α, and the subsequent terms are constraint penalty terms. The term $\gamma_3|SOC(t_f) - SOC_{\text{target}}|$ is necessary to eliminate trivial solutions (in which the cell is not charged at all), and is chosen in favor of a higher-order penalty term (e.g., $|SOC - SOC_{\text{target}}|^2$) to penalize any deviation from the target SOC, without relaxing the constraint as long as the target SOC is not reached.

The terms $\epsilon_i \log f_i$ in (11a) are chosen to enforce the first five inequality constraints listed in (11b). Precisely, the functions f_i are chosen to be

$$\begin{aligned} & f_1 = \min_{t,j}\left(c_{s,n}^{(j)}/c_{s,n,\min} - 1\right), f_2 = \min_{t,j}\left(1 - c_{s,n}^{(j)}/c_{s,n,\max}\right) \\ & f_3 = \min_{t,j}\left(c_{s,p}^{(j)}/c_{s,p,\min} - 1\right), f_4 = \min_{t,j}\left(1 - c_{s,p}^{(j)}/c_{s,p,\max}\right) \\ & f_5 = \min_{t}(1 - V_{\text{cell}}/V_{\max}). \end{aligned} \tag{12}$$

The inclusion of the logarithm function ensures that the value of J is only for paths in the feasible set, and smoothly penalizes solutions close to the boundary of the feasible set.

Values used for the scaling parameters in (11a) are shown in Table II. The values of γ_1 and γ_2 were chosen to bring the objective terms to roughly the same order of magnitude. The value of γ_3 was chosen to be sufficiently large, without adversely affecting the optimizer performance. The parameters $\epsilon_1, \ldots, \epsilon_5$ are only required to be positive, and the value shown in Table II were verified to have insignificant impact on the solution.

TABLE II
VALUES OF SCALING PARAMETERS

Quantity	Value	Quantity	Value
γ_1	2×10^{-2}	ϵ_2	10^{-4}
γ_2	5×10^{9}	ϵ_3	10^{-4}
γ_3	10^{5}	ϵ_4	10^{-4}
ϵ_1	10^{-4}	ϵ_5	10^{-4}

The numerical approach we follow here to tackle the OCP (11a) subject to (11b) is a discretize-then-optimize strategy. Because the states describing the battery evolve over disparate timescales (e.g., electrochemical timescales versus temperature timescales), using a single discretization scheme for both state and control may result in a chattering control signal that fluctuates on the shortest timescale. This fluctuation may be undesirable due to hardware limitations, motivating a numerical approach that discretizes the control and the state separately. We begin by discretizing the control signal I piecewise on the set of intervals $\{[SOC_0, SOC_1], [SOC_1, SOC_2], \ldots, [SOC_{N-1}, SOC_N]\}$, where N is the number of intervals over which the

piecewise control is defined, distinct from subscripted N_{total}, which refers to the length of the state vector. While it is intuitive to divide the control signal based on time intervals $\{[0, t_1], [t_1, t_2], \ldots [t_{N-1}, t_f]\}$, the latter strategy requires a priori knowledge of t_f, which is one of the objects of search. Furthermore, using $\{[0, t_1], [t_1, t_2], \ldots [t_{N-1}, t_N]\}$ with arbitrarily defined t_N introduces an additional numerical parameter, such that any control and state data beyond $t = t_f < t_N$ is of little relevance to the OCP.

The control current I is discretized piecewise as

$$I(SOC) = \sum_{j=0}^{p} \beta_{i,j} \phi_j (SOC - SOC_i),$$
$$SOC \in [SOC_i, SOC_{i+1}] \tag{13}$$

for $i = 0, 1, \ldots, N-1$, where ϕ_j are chosen basis functions, $\beta_{i,j}$ are the corresponding coefficients, and p is the order of the basis. In general, the basis functions are chosen a priori to reflect desired properties such as periodicity or smoothness (continuity, differentiability, etc.). In particular, periodic basis functions can be chosen for simulating multiple charge and discharge cycles to investigate the long-term degradation of the cell. The scope of this letter is limited to a single charging cycle, and as such, only piecewise polynomials will be considered for simplicity. Let $\phi_j(x) = x^j$ be the polynomial basis functions. In the following, we will consider $p = 0, 1, 2$, which are respectively the piecewise constant, piecewise linear and piecewise quadratic basis functions. To reduce the problem dimension and obtain smoother control signals, we enforce continuity for $p = 1$ and continuity of the derivative for $p = 2$. Note that constructing smooth control signals this way eliminates the need to explicitly handle chattering in the objective function, as is necessary in MPC [8]. An initial guess I_{guess} for the control in the chosen basis is supplied as a vector of parameters $\mathbf{b}_0 = [\beta_{0,1}, \ldots, \beta_{N-1,p}]$. The initial guess is distinct from the initial condition or initial state of the system; the latter concerns the state at $t = 0$, while the former is a function defined over $[0, t_f]$ that serves as a starting point for the iterative optimization algorithm. Note that for $p = 0, 1$, and 2, smoothness constraints imply that the dimension of the vector $\mathbf{b}$ is $N, N+1$, and $N+2$ respectively. In the absence of a priori information on the optimal current, we will consider only initial guesses corresponding to a constant current at an amplitude I_0, i.e., $I_{\text{guess}}(t) = I_0$ for $t \in [0, t_f]$. The present discretization strategy reduces the OCP to the nonlinear program (NLP) in which we seek $\mathbf{b}^* \in \mathbb{R}^{N+p}$ and the corresponding control current I^* so that

$$\mathbf{b}^* = \underset{\mathbf{b}}{\operatorname{argmin}}\, J(\mathbf{b}) \tag{14}$$

such that

$$I_{\min} \leq I^*(t) \leq I_{\max} \tag{15}$$

for $t \in [0, t_f]$. Beginning from the initial guess $\mathbf{b}_0$, the value of $J(\mathbf{b}_{\text{init}})$ and the numerical gradient of J are computed via numerical solution of the governing ODEs. Subsequently, a new iterate $\mathbf{b}_1$ is produced by the NLP solver, which is then used to compute $J(\mathbf{b}_1)$, and so on. The interior point method [16] from MATLAB's `fmincon` package is used to solve the constrained NLP. The ODE solver `ode15s` [17] based on a modification of the backward differentiation formulae (BDF) is chosen here for its suitability for stiff ODE systems. The additional termination event $SOC = SOC_{\text{target}}$ is provided to the solver to ensure the solver stops at $t = t_f$.

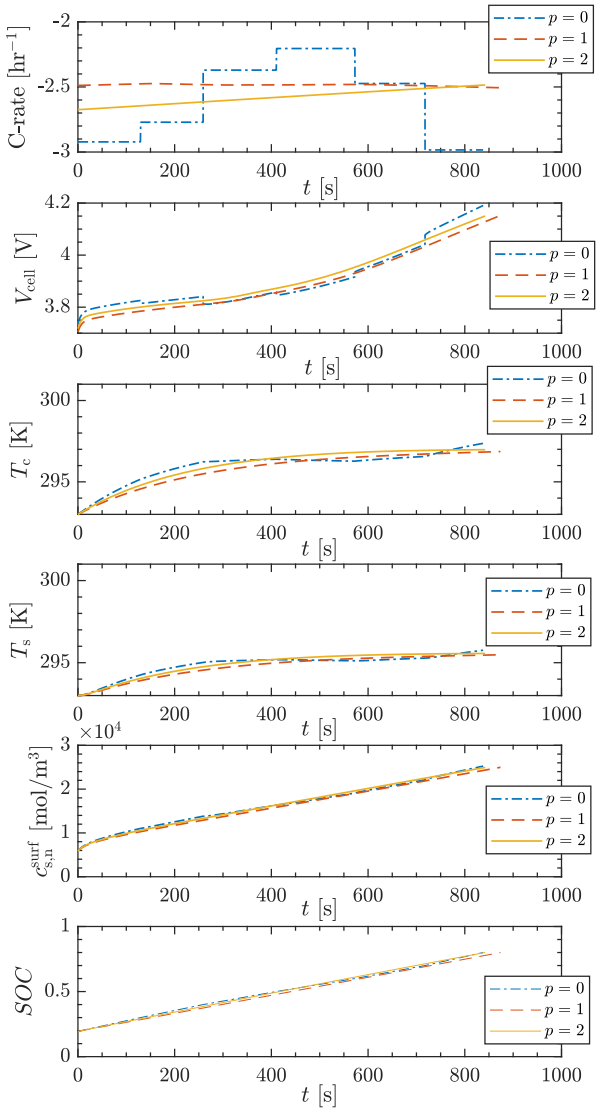

Fig. 1. Key states, including the C-rate (current normalized by nominal capacity), shown as a function of time, using $\alpha = 0.1$, and $N = 6$.

IV. Results and Discussion

The optimal current profile is presented in terms of C-rate I^*/Q in Fig. 1, along with the cell voltage, the core temperature, the surface temperature, the anode surface concentration, and the state of charge. Depicted curves correspond to $p = 0, 1$, and 2, with $T_{\text{amb}} = 293$ K, $\alpha = 0.1$, and $N = 6$. Throughout, a constant current profile with $I_0 = -5$ A (-2.5C) is provided as an initial guess unless otherwise specified. The problem described by this set of parameters is multi-objective, since the solution sought minimizes a weighted combination of charging time and aging (described by SEI layer thickness). Note that the $p = 0$ result

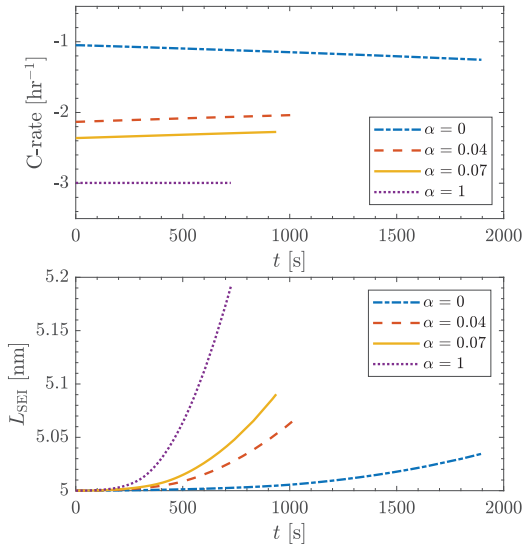

Fig. 2. Optimal current profiles and the corresponding evolution of L_{SEI} for $p = 2$ and $N = 6$.

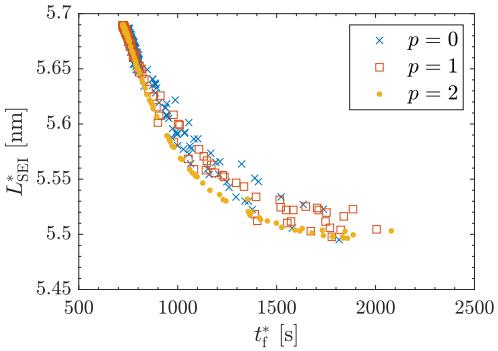

Fig. 3. Pareto front showing the tradeoff of SEI layer objective L^*_{SEI} and charging time t^*_{f} for $p = 0, 1, 2$.

can be interpreted as N constant current stages of a CC-CV charging protocol. In this letter, $SOC_{\mathrm{target}} = 0.8$, so the constant voltage stage can be assumed to begin at the optimization horizon at $SOC = 0.8$.

For each case of p in Fig. 1, the same optimal objective value of $J^* = 24.7$ is attained, and a similar evolution is observed in all cases for the surface concentration and state of charge. For $p = 0$ the optimal current profile differs significantly from the $p = 1$ and $p = 2$ cases, achieving a faster charging time ($t_{\mathrm{f}} = 838$ s) but greater aging ($L_{\mathrm{SEI}}(t_{\mathrm{f}}) - L_{\mathrm{SEI}}(0) = 0.111$ nm) compared to, for example, the $p = 1$ case ($t_{\mathrm{f}} = 874$ s; $L_{\mathrm{SEI}}(t_{\mathrm{f}}) - L_{\mathrm{SEI}}(0) = 0.109$ nm).

The optimal current profile for $p = 2$ and varying α is shown in Fig. 2, where $\alpha = 0$ corresponds to minimizing only aging, and $\alpha = 1$ corresponds to minimizing only charging time. The intermediate values of $\alpha = 0.04$ and $\alpha = 0.07$ are chosen for the sake of exposition as balanced optimization cases. Choosing $\alpha = 1$ implies that the solution, as expected, is the constant charging current of maximum amplitude ($I = I_{\mathrm{min}} = -6$ A). Correspondingly, the growth of the SEI layer is far quicker than the other cases, as depicted in Fig. 2. Note that because the interior point method is used as an optimization method, the optimal charging profile computed

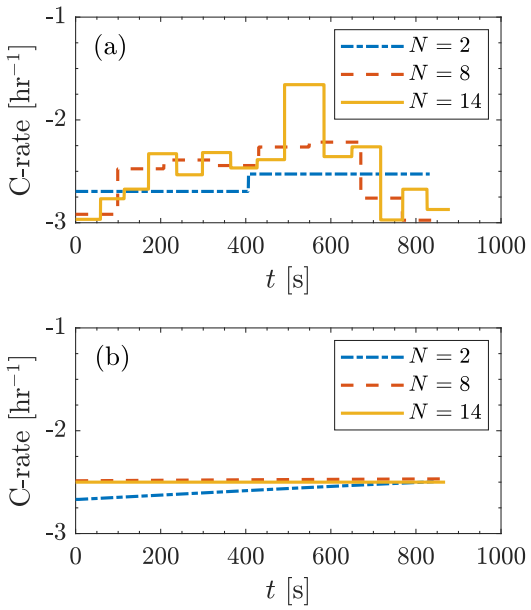

Fig. 4. Optimal current profiles for $N = 2$, 8, and 14, and $\alpha = 0.1$ with (a) $p = 0$, and (b) $p = 2$.

satisfies $I(t) > I_{\mathrm{min}}$ for all t. On the other hand, choosing $\alpha = 0$ results in a charging current profile that gradually increases in magnitude over time. Because the aging model is calibrated on data that captures both cycle aging and calendar aging, the optimal charging current is not the minimal magnitude solution (i.e., $I = I_{\mathrm{max}} = -0.5$ A) but rather an intermediate level of current that finishes charging in a reasonable amount of time. Indeed the growth of L_{SEI} shown in Fig. 2 for $\alpha = 0$ accelerates later in the charging process. Choosing $\alpha = 0.04$ or $\alpha = 0.07$ results in a charging profile that lies between the two extreme cases, with the magnitude of I staying relatively constant. The tradeoff between the optimal value t^*_{f} of charging time and the optimal value L^*_{SEI} of SEI layer at $t = t_{\mathrm{f}}$ is summarized in the Pareto front depicted Fig. 3. Each marker corresponds to one optimization run, with different-shaped markers corresponding to different values of p. While the markers for $p = 0$ and $p = 1$ display some scatter, the markers for $p = 2$ delineate a smooth front, achieving the best values of t^*_{f} for fixed L^*_{SEI} and vice versa. The superior results from using $p = 2$ suggest that in general, enforcing smoothness in the control current results in more consistent solutions than the simpler, piecewise constant control.

Notably, for low values of t^*_{f} in Fig. 3, all values of p produce similar values of L^*_{SEI}, since the optimal current produced in each case is approximately the constant profile at maximum amplitude. In contrast, for low values of L^*_{SEI}, a large scatter in solution performance is observed for $p = 0$ and $p = 1$. The strong parameter dependence for the $p = 0$ case is contrasted with the relative robustness of $p = 2$ in Fig. 4. In Fig. 4(a), $p = 0$ solutions are shown for various interval counts N, with the resulting solutions being vastly different. The $p = 2$ solutions in Fig. 4(b), however, change little as N is increased. Computational cost increases as p is increased, due to a slight increase in the number of degrees of freedom and the requirement of handling higher degree polynomials while

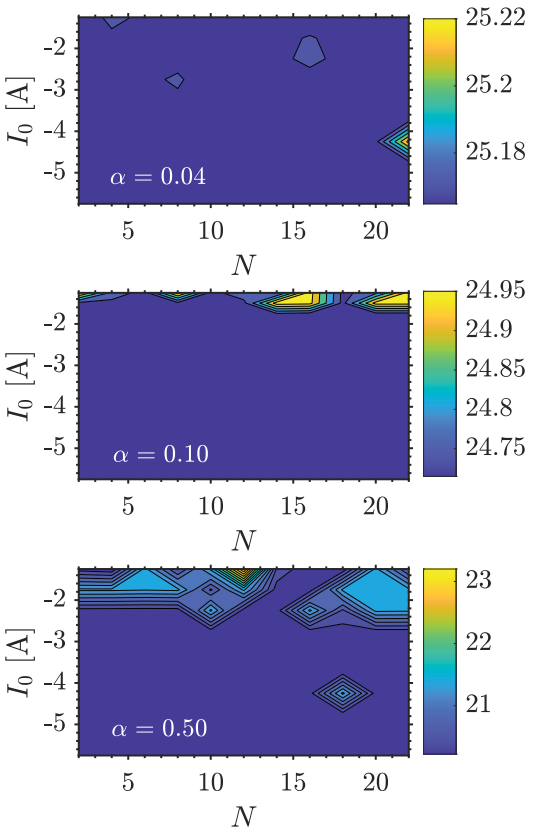

Fig. 5. Contour plot of optimal objective function value J^* with varying numerical parameters I_0 and N, for $p = 2$.

enforcing the continuity constraint. The computational cost is also strongly dependent on N, which can be changed without compromising accuracy of the ODE approximation (i.e., the chosen numerical solver of the ODE). Fig. 5 shows contours of the optimal objective function value J^* in the space of N and I_0, demonstrating the independence of J^* over these numerical parameters. Here $p = 2$, and $\alpha = 0.04$, 0.1, and 0.5. Note the different color scales used to resolve the contours. For values of I_0 close to the upper bound $I_{\max}$, the solution quality is notably degraded. Nonetheless, choosing values of I_0 well in the interior of $[I_{\min}, I_{\max}]$ gives a solution robust to I_0 and N. Notably, a small value of N is sufficient to obtain a good solution in this multiobjective setting, suggesting feasibility of a future online implementation. By replacing the detailed electrochemical-thermal-aging model used in this letter with a simple ROM—which is straightforward thanks to the decoupling of the control and state discretizations in this optimal control framework—one may freely adjust the complexity and computational cost of this model. While the wall clock time of each optimization run is dependent on the initial guess, the converged current profile varies little as a function of initial guess, suggesting that the solution method is robust to the choice of numerical parameters. Furthermore, the computational cost of the present approach scales more slowly than, say, collocation-based methods, since the numerical Hessian matrices in this framework (required by the interior point method) have size $(N+p) \times (N+p)$, independent of the PDE discretization accuracy.

V. Conclusion

The results of applying the direct single shooting optimal control framework to a fully coupled electrochemical-thermal-aging model with a large number of states were presented. Polynomial bases with varying degree p were used, and the robustness of continuous, differentiable piecewise quadratic control ($p = 2$) was identified, in contrast to the commonly used piecewise constant current control ($p = 0$). While the present numerical approach requires careful handling of path constraints via penalty terms, the strengths of this approach include the low dimensionality of the resulting NLP despite stiff dynamics that may require fine timesteps, and the ability of the user to control the desired properties of the control signal such as continuity via choice of basis functions. Furthermore, the structure of the optimal control framework (discretize-then-optimize) allows quick integration with different battery models of increasing complexity for greater fidelity, or with reduced order models to facilitate online implementation and subsequent experimental validation.

References

[1] B. Scrosati and J. Garche, "Lithium batteries: Status, prospects and future," *J. Power Sources*, vol. 195, no. 9, pp. 2419–2430, 2010.
[2] D. Lisbona and T. Snee, "A review of hazards associated with primary lithium and lithium-ion batteries," *Process Safety Environ. Protection*, vol. 89, no. 6, pp. 434–442, 2011.
[3] A. Abdollahi *et al.*, "Optimal battery charging, part I: Minimizing time-to-charge, energy loss, and temperature rise for OCV-resistance battery model," *J. Power Sources*, vol. 303, pp. 388–398, Jan. 2016.
[4] H. E. Perez, X. Hu, S. Dey, and S. J. Moura, "Optimal charging of li-ion batteries with coupled electro-thermal-aging dynamics," *IEEE Trans. Veh. Tech.*, vol. 66, no. 9, pp. 7761–7770, Sep. 2017.
[5] B. Suthar, P. W. Northrop, R. D. Braatz, and V. R. Subramanian, "Optimal charging profiles with minimal intercalation-induced stresses for lithium-ion batteries using reformulated pseudo 2-dimensional models," *J. Electrochem. Soc.*, vol. 161, no. 11, 2014, Art. no. F3144.
[6] R. Methekar, V. Ramadesigan, R. D. Braatz, and V. R. Subramanian, "Optimum charging profile for lithium-ion batteries to maximize energy storage and utilization," *ECS Trans.*, vol. 25, no. 35, p. 139, 2010.
[7] R. Klein, N. A. Chaturvedi, J. Christensen, J. Ahmed, R. Findeisen, and A. Kojic, "Optimal charging strategies in lithium-ion battery," in *Proc. Amer. Control Conf. (ACC)*, 2011, pp. 382–387.
[8] C. Zou, X. Hu, Z. Wei, T. Wik, and B. Egardt, "Electrochemical estimation and control for lithium-ion battery health-aware fast charging," *IEEE Trans. Ind. Electr.*, vol. 65, no. 8, pp. 6635–6645, Aug. 2018.
[9] M. A. Xavier, *Efficient Strategies for Predictive Cell-Level Control of Lithium-Ion Batteries*, Univ. Colorado, Boulder, CO, USA, 2016.
[10] M. Xu, R. Wang, P. Zhao, and X. Wang, "Fast charging optimization for lithium-ion batteries based on dynamic programming algorithm and electrochemical-thermal-capacity fade coupled model," *J. Power Sources*, vol. 438, Oct. 2019, Art. no. 227015.
[11] M. Song and S.-Y. Choe, "Fast and safe charging method suppressing side reaction and lithium deposition reaction in lithium ion battery," *J. Power Sources*, vol. 436, Oct. 2019, Art. no. 226835.
[12] M. M. Martín, *Introduction to Software for Chemical Engineers*. Boca Raton, FL, USA: CRC Press, 2014.
[13] T. Weaver, A. Allam, and S. Onori, "A novel lithium-ion battery pack modeling framework-series-connected case study," in *Proc. Amer. Control Conf. (ACC)*, 2020, pp. 365–372.
[14] E. Prada, D. Di Domenico, Y. Creff, J. Bernard, V. Sauvant-Moynot, and F. Huet, "A simplified electrochemical and thermal aging model of liFePO$_4$-graphite li-ion batteries: Power and capacity fade simulations," *J. Electrochem. Soc.*, vol. 160, no. 4, p. A616, 2013.
[15] M. Pathak, D. Sonawane, S. Santhanagopalan, R. D. Braatz, and V. R. Subramanian, "Analyzing and minimizing capacity fade through optimal model-based control-theory and experimental validation," *ECS Trans.*, vol. 75, no. 23, p. 51, 2017.
[16] R. H. Byrd, J. C. Gilbert, and J. Nocedal, "A trust region method based on interior point techniques for nonlinear programming," *Math. Program.*, vol. 89, no. 1, pp. 149–185, 2000.
[17] L. F. Shampine and M. W. Reichelt, "The MATLAB ODE suite," *SIAM J. Sci. Comput.*, vol. 18, no. 1, pp. 1–22, 1997.